Chapter 6

Neutron Dose Equivalent in Tissue Due to Linacs of Clinical Use

S. Agustín Martínez Ovalle

Additional information is available at the end of the chapter

http://dx.doi.org/10.5772/56513

1. Introduction

When operating linear accelerators of clinical use at energies above 8 MeV, neutrons are produced when either electron or photon configurations are used [1]. This is mainly due to the interactions of photons and electrons of such energies with the high-Z materials present in the accelerator head (target, scattering foils, collimators, etc.) [22]. Because of their high relative biological effectiveness, photoneutrons are a particular source of unwanted out-of-field exposure of patients and several authors have pointed out the possibility of associated risks of secondary cancers after radiotherapy.

The overdose due to neutrons in patients undergoing radiotherapy is difficult to measure or estimate. Neutron fluence and spectra in water have been measured using bubble detectors and superheated drop detectors [8, 9, 21], ^{197}Au-based Bonner spheres [12] and thermoluminescent dosemeters [11, 35, 40]. [10] measured the neutron fluence at the patient plane for various linacs using gold-foil activation. [13], using the same technique, measured neutron spectra for various linacs and determined neutron fluence and ambient dose equivalents. All these measurements offer valuable information that can be compared with the results of Monte Carlo simulations.

The Monte Carlo simulation has been used to study different problems linked to neutron dosimetry. [18] calculated neutron fluence and spectra at different positions surrounding a Varian Clinac 2100C/2300C linac. [31] studied the production of neutrons in the high-Z components of a Siemens Mevatron linac. [7] investigated the field size effects, off-axis dose profiles, neutron contribution from the linac head, and dose contribution from capture gamma rays, phantom heterogeneity effects and effects of primary electron energy shift in some Linac configurations. [41] calculated neutron ambient dose equivalent for different collimator configurations in a Varian Clinac 2300 C/D. [34] studied the effects of modeling different accelerator head and room geometries on the neutron fluence and spectra for a Siemens Primus Linac. [3] determined neutron doses to critical organs for a Siemens Mevatron KDS. Different versions of the Monte Carlo N-particle transport code [5] were used in all these works. Recently [37], dose to patients due to the emitted photoneutrons were calculated by

carrying out the simulations with Geant4 [2], the latest generation of the old Geometry and Tracking (GEANT) Monte Carlo code.

Even the Electron Gamma shower (EGS) Monte Carlo code, in particular EGS4 [30], was used to investigate neutron sources in a Varian Clinac [23].

Despite the large amount of calculations available, there is not much information about the increase in the dose to patients due to neutrons produced in the linac head. Only very recently, a detailed study was carried out by [19], who calculated neutron spectra and dose equivalent in tissue for a Varian Clinac.

Another problem occurring with the previous works is that neutron fluence and doses in radiotherapy were analyzed with different methodologies, for various Linacs, patient or phantom models, energies, field sizes, gantry angles, treatment modes etc. As a consequence, the results obtained until now have significant differences between them as some authors have pointed out [11, 21, 40].

The neutron contribution yielded by some linacs commonly used for radiotherapy was evaluated using the Monte Carlo code MCNPX (v. 2.5) [33]. Eight different configurations for linacs of three different manufacturers have been considered. The approach includes two main points. First, the various linacs have been analyzed using the same methodology, thus permitting a meaningful comparison between the results obtained. Secondly, we have focused on the dose to patients. Thus, we have calculated neutron fluence, neutron spectra, absorbed dose and dose equivalents in various points of an ICRU tissue phantom. The results from studies done in this chapter have led to several publications [24–26, 36].

2. ICRU tissue phantom

The phantom used in all cases, a phantom of $100 \times 50 \times 30$ cm^3, made of ICRU tissue (11 % Carbon, 76.2 % Oxygen, 10.1 % Hydrogen and 2.6 % Nitrogen in weight) [16], simulating a patient was situated with its surface at 100 cm from the source. The Fig. 1 shows schematically the phantom half, as used in the simulations.

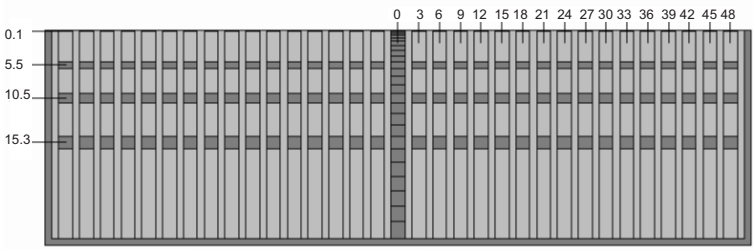

Figure 1. Outline of 1/2 ICRU phantom indicating the position of the cells in direction at axis Z radiation and outside the axis.

Dark gray cells are the positions where the neutron determinations and shown correspond to the axis and transverse positions situated off axis, between 0 and 48 cm, and 0.1, 5.5, 10.5 and 17.1 cm deep. In order to improve the statistical distribution of the cells with depth in the radiation beam axis increases proportionally with the depth from $2.0 \times 2.0 \times 0.1$ cm^3, in the surface, to $2.0 \times 2.0 \times 2.4$ cm^3, in deep.

3. Description of linacs

We studied three brands of accelerators. The simulated models correspond to the linacs Varian Clinac 2100C/D for configurations of 10, 15, 18, and 20 MV, Elekta Inor of 15 MV Elekta SL-25 18 MV and Siemens KDS 18 MV. The geometries were constructed according to manufacturer's specifications and following some recommendations from previous work. Both the jaws as the system multileaf (MLC) were fitted in all cases to achieve a treatment field of 10×10 cm^2, with which all simulations were performed.

		Siemens KDS	Elekta Inor	Elekta SL25	Varian Clinac	
		18 MV	15MV	18 MV	15 MV	18/20 MV
target	materials	Au	W/Re	W/Ni/Fe	W	
	[%]	100	90/10	95/3.75/1.25	100	
	ρ [g cm^{-3}]	19.3	19.4	18.0	19.3	
target	materials	Cu	Cu		Cu	
cover	[%]	100	100		100	
	ρ [g cm^{-3}]	8.96	8.96		8.96	
primary	materials	W	W/Ni/Fe	Pb/Sb	W	
collimator	[%]	100	95/3.75/1.25	96/4	100	
	ρ [g cm^{-3}]	19.3	18.0	11.12	19.3	
flattening	materials	Cr/Fe/Ni	Cr/Ni/Fe		W	Ta/Fe
filter	[%]	18/74/8	18/74/8		100	–
	ρ [g cm^{-3}]	8.03	8.03		19.3	16.65/7.874
secondary	materials	W	W/Ni/Fe	Pb/Sb	W	
collimator	[%]	100	95/3.75/1.25	96/4	100	
	ρ [g cm^{-3}]	19.3	18.0	11.12	19.3	
multileaf	materials		W/Ni/Fe	Pb/Sb	W	
collimator	[%]		95/3.75/1.25	96/4	100	
	ρ [g cm^{-3}]		18.0	11.12	19.3	
jaws	materials	W	W/Ni/Fe	Pb/Sb	W	
	[%]	100	95/3.75/1.25	96/4	100	
	ρ [g cm^{-3}]	19.3	18.0	11.12	19.3	

Table 1. Materials of the various elements of the linac heads considered in this work. The percentage compositions and densities, ρ, are also given. The Varian Clinac flattening filter for 18 and 20 MV is made of Ta with a cover of Fe.

The differences between marks of accelerators, are primarily concerned with the materials used in the construction of each of the parts of the head of the linacs, as the target for X-ray production, which is usually embedded within a shell material which is usually Cu, the flattening filter or filters, with some models of those studied here compose of a double filter flatter built of different materials depending on the marks, the MLC and the jaws, which are usually constructed of W, and the outer shield , which is usually of Pb and Fe. All these components, are responsible of the production of neutrons in the head of the accelerator. The materials that make up each of these elements and their densities for the accelerators studied here are summarized in Table 1.

The evaluation of this production cannot be neglected if one considers that these devices produce neutrons to the order of 1012 neutrons per Gy in conventional radiotherapy treatment [10]. Furthermore it has been demonstrated in previous studies [23]; [34]; [22] that in fact, neutron production is defined by the material used and its respective threshold to the photonuclear reactions. For example, it is noted that Varian models used materials (see Table

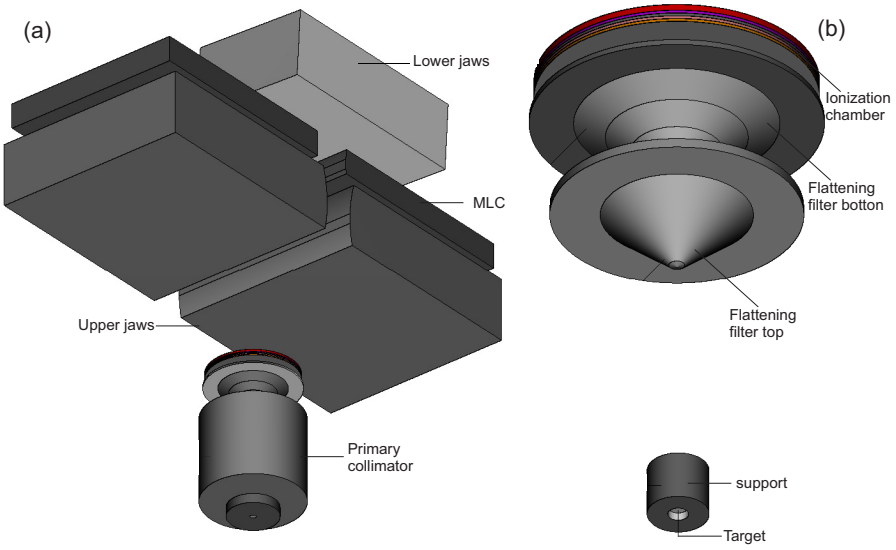

Figure 2. Geometry of an Elekta accelerators.

1), with Z higher than those used by other models for the construction of the head. This aspect will be reflected in the production of neutrons of the Linacs.

The mechanism that allows the generation of neutrons, is mainly the reaction (γ, n), which depends on the energy of the photons incident on these materials. The threshold energy of the incident photon to produce this type of reaction is 7.6, 6.2, 6.7, 13.1, 7.6 and 8.1 MeV for Ta, W, Pb, Al, Fe and Au, respectively [27], which are the main components of the target, flattening filter, jaws, MLC systems and shield of different teams studied. This means that the photoproduction mechanism is fully guaranteed for accelerators with energies above 10 MV.

Fig. 2a shows the geometry of an Elekta accelerator. These geometries correspond the Inor model of 15 MV and SL25 of 18 MV, in this case, the geometries of the two models have the same characteristics in terms of dimensions of the various elements; the differences are in the materials used in construction of the target, MLC system and jaws as seen in Table 1. Fig. 2b shows the target (1 mm in diameter) and target cover of Cu with the dual flattening filter system, constructed of stainless steel.

Each of the accelerators studied requires a previous tuning process, in order to establish the energy of incident electrons, to make it suitable for calculations. This process is carried out by comparison between the curves of percentage depth dose (PDD) simulated and measured, the latter provided by each of the radiophysics services from hospitals in which the respective model is studied. However, for models Varian Clinac 2100 C/D of 10 MV and 20 MV, it was not possible to get the experimental PDD.

The process starts by estimating the energy values around the nominal energy value of the accelerator. For each of these energies: $TPR_{20,10}$ maguitude is calculated. Which is the amount recommended by dosimetry protocols based on both air kerma patterns, as in patterns of absorbed dose in water [14, 17, 39]. This quantity is defined as the ratio between the absorbed

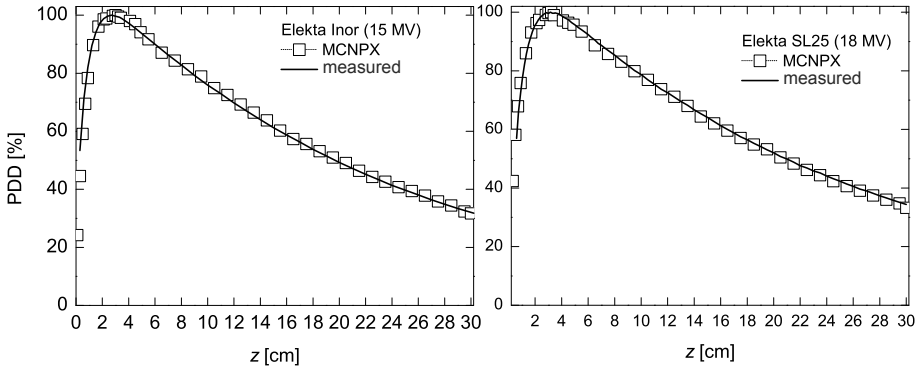

Figure 3. Comparison of PDD's calculated with MCNPX for Inor Elekta accelerators of 15 MV (left) and Elekta SL 25 of 18 MV (right) with those measured experimentally.

dose in the beam axis at 20 cm and 10 cm deep in a water phantom, obtained with a source detector distance constant of 100 cm and a field size 10×10 cm^2 in the position of the detector.

Having determined the values of $TPR_{20,10}$ to the energies considered, a calibration curve is established and from the experimental value of $TPR_{20,10}$ a tuning energy is obtained. Fig. 3 compares the experimental PDD, that were measured in hospitals Ramón and Cajal of Madrid (Spain) and Hospital Río Hortega of Valladolid (Spain), with those obtained after tuning to Inor Elekta accelerators of 15 MV and 18 MV SL-25. As we see the agreement is excellent.

The value of the maximum dose due to photons supplied by the accelerator in the build-up region is extacted from the simulated PDD. In the case of Elekta accelerators, these maximum values are 6.06×10^{-16} y 1.09×10^{-15} Gy of photons emitted per electron, and are at 3.0 and 3.2 cm depth, respectively. These depths are in good agreement with those published in the [4], for accelerators of this energy. The dose values found in the build-up region are the value reference against which the dose equivalent due to photoneutrons is expessed.

Let's say in conclusion that for Elekta models, the electron beam incident on the target is simulated by a Gaussian of mean value 13.77 MeV and 0.8 MeV of FWHM for the Elekta Inor, and 16.1 MeV and 1.5 MeV for the Elekta SL-25.

The next accelerator that was studied is the Siemens Mevatron KDS in configuration of 18 MV (Fig. 4), the electron beam that impinges on the target (also of 1 mm diameter) was simulated using a Gaussian of average value of 15.5 MeV and 1.5 MeV of FWHM. This energy is selected, Based on the previous tuning of the accelerator by means of the experimental PDD and was provided by the Hospital Universitary St. Cecilio of Granada (Spain) (Fig. 5). The maximum dose due to photons supplied in the region of the build-up is de 4.48×10^{-15} Gy of photons per emitted electron and is 3.2 cm deep.

The last accelerator studied and one of the most commonly found with dual energies of 6 and 15 MV or 6 MV and 18 MV, is the accelerator Varian Clinac 2100 C/D. Fig. 6 shows the geometry corresponding to the configurations of 10, 15, 18 and 20 MV of photons. In this case the electron beam incident on the target of 1 mm diameter is simulated, respectively, by a monodirectional and monoenergetic beam of 10.5, 15.04, 18.3 and 20.5 MeV. These energies are obtained in tuning of each of the accelerators, by comparison with experimental PDDs,

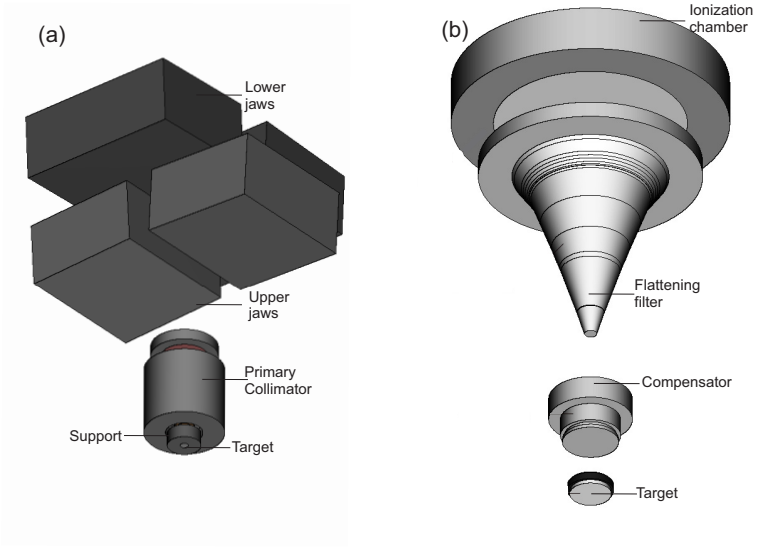

Figure 4. Geometry accelerator Siemens KDS of 18 MV.

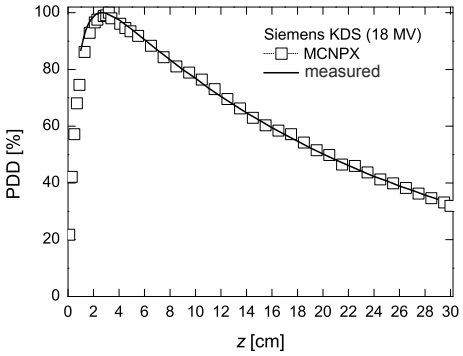

Figure 5. Comparison of PDD calculated with MCNPX for accelerator Siemens KDS of 18 MV and measured experimentally.

which were supplied by the Hospital Clinic Universitary of Valladolid (Spain) (for 15MV) and the Hospital Virgin of the Nieves in Granada (Spain) (for 18 MV).

The energies of tuning for the accelerator 10 and 20 MV were taken from [23], who simulated these models. The maximum dose due to photons in these accelerators in the build-up region are 2.78×10^{-16}, 4.85×10^{-16}, 6.57×10^{-16} and 1.18×10^{-15} Gy of photons per emitted electron, and are at 2.8, 3.0, 3.2 and 3.4 cm depth, respectively, for the four configurations analyzed.

In Fig. 6a, the geometry maintains the same dimensions for the four configurations studied, except for materials used in the manufacture of components (see Table 1). Fig. 6b shows, the target and your cover and the flattening filter. These accelerators are equipped with MLC

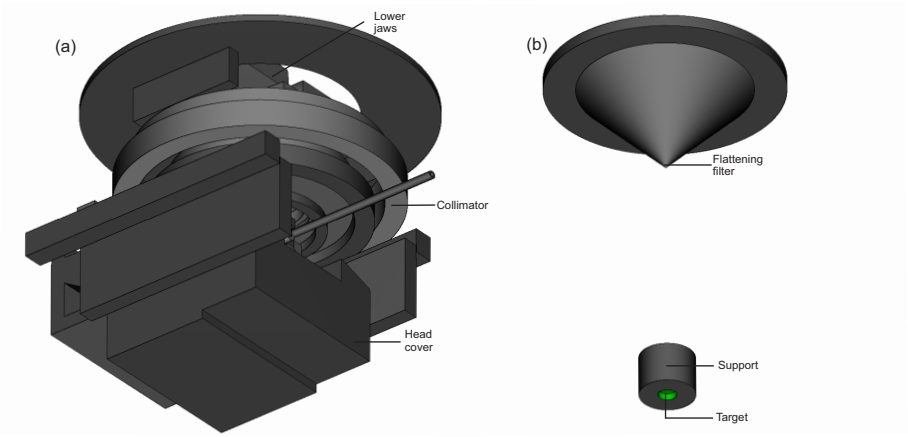

Figure 6. Geometry the accelerators Varian Clinac 2100 C/D.

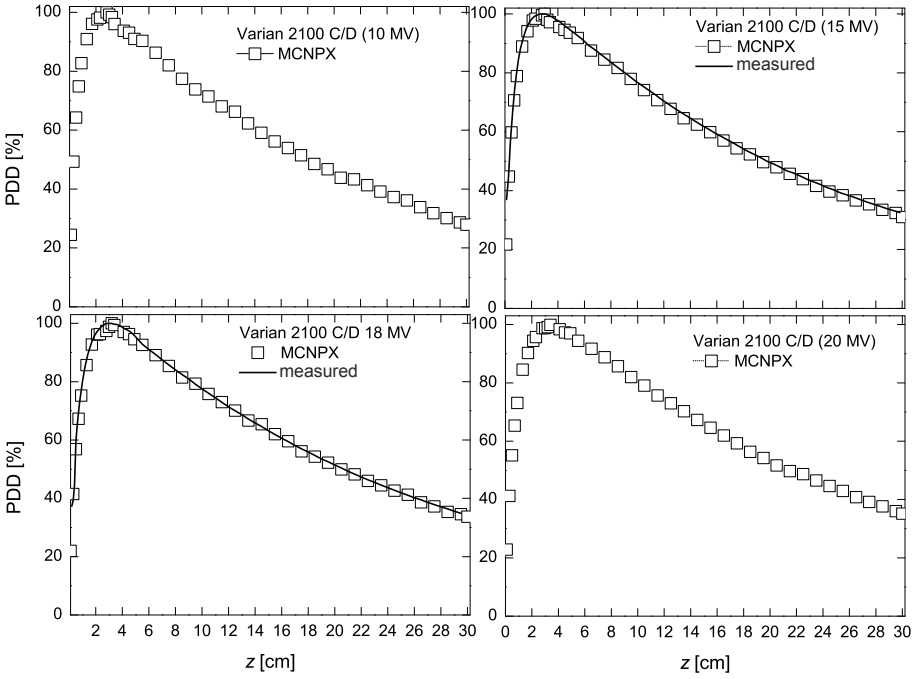

Figure 7. Comparison of PDD calculated with MCNPX for accelerators Varian Clinac 2100 C/D of 10, 15, 18, and 20 MV and the measured experimentally for 15 and 18 MV.

system, similar to the Elekta models studied. Fig. 7 shows the different PDD's of tuning for each Varian accelerators studied

In this case, the geometry used for the simulations was constructed from 93 geometric elements which include cones, cylinders, spheres, truncated cones, parallelepiped, triangular

prisms, pyramids triangular, and quadrangular pyramids. In the simulations the Elekta accelerators, the shielding cover of Varian accelerator was included, because it was not possible to obtain data on the dimensions of the shielding cover of Elekta accelerator, considering that the materials used by different manufacturing for shielding the head are similar. wherever the shielding cover is not included we have called it geometry simplified in contradistinction is full geometry where the shielding cover is included.

The objective to study simplified and full geometries is due to the different positions opposing about the shielding against neutron radiation. Works like of the [23] established minimal differences in using of simplified geometries and complete for calculating photoneutrons. This has led most authors to use simplified geometries in their calculations [32]; [20]; [7]; [42]; [34]; [3]; [28]. Taking advantage that we have the complete geometry of the accelerator Varian Clinac 2100 C/D, we have studied the influence of the shielding cover in this study.

4. Monte Carlo simulation

As noted above, once the tuning of each accelerator, was held from the simulated PDD, the depth at which it obtain the maximum absorbed dose due to photons in the region of the build-up was determinated. This value is used as reference to express all the calculations reported here for neutron dosimetry.

4.1. Neutron fluence in ICRU tissue phantom

The fluence of neutron in each accelerator is initially calculated as a function of depth into the phantom and on the axis of central radiation.

Fig 8 shows the results of fluence for the six accelerators studied. The white squares correspond to the Varian accelerators, the black circles to the Elekta accelerators and the white circles to the Siemens accelerators. The results have been grouped in each panel according to energy. As seen, the shape of the fluence curve as a function of depth on the phantom is similar in all accelerators. The differences between them are summarized in Table 2, showing the highest values of fluence, Φ_{max} and depth at which this maximum is reached, d_{max} . As we see, this depth varies between 2.03 and 2.55 cm in all cases except for the Elekta SL-25 of 18 MV for which the maximum is at 3.61 cm.

linac	Φ_{max} [cm^{-2}]	d_{max} [cm]
Siemens KDS 18 MV	$0.37 \cdot 10^{-8}$	2.20
Elekta Inor 15 MV	$0.39 \cdot 10^{-8}$	2.55
Elekta SL25 18 MV	$2.07 \cdot 10^{-8}$	3.61
Varian Clinac 15 MV	$1.46 \cdot 10^{-8}$	2.32
Varian Clinac 18 MV	$3.25 \cdot 10^{-8}$	2.03
Varian Clinac 20 MV	$5.30 \cdot 10^{-8}$	2.22

Table 2. Maximum fluence per emitted electron, Φ_{max}, and depth at which this maximum is reached, d_{max}, for the various configurations and linacs studied.

The maximum fluence of neutron, increases with the energy in accelerators of the same model. The maximum fluence is seen in the Varian 20 MV and is 1.6 times greater than in the Varian 18

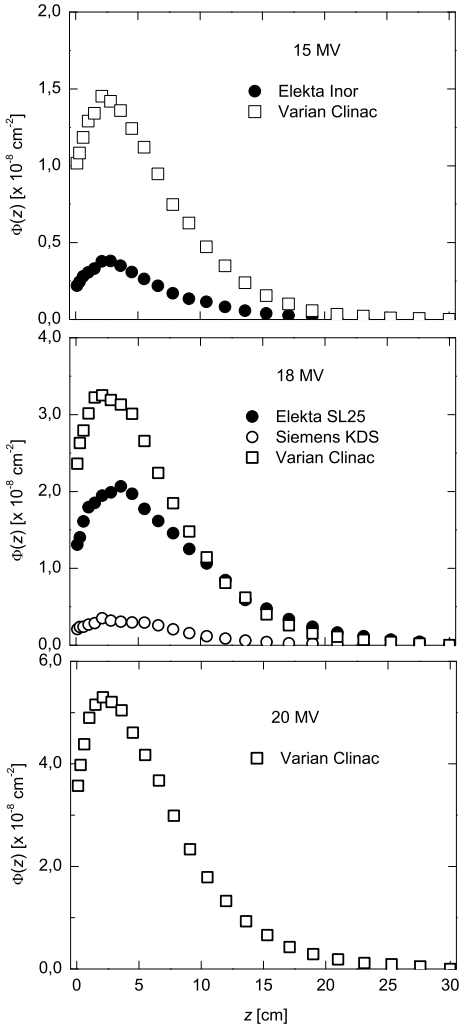

Figure 8. Neutron fluence by electron emitted as a function of depth in phantom of ICRU tissue for each of the accelerators. $Z = 0$ corresponds to the surface of the phantom.

MV, while that in Varian 18 MV it is 2.2 times greater than in the Varian 15 MV. The difference is even greater among Elekta, in which the maximum fluence of SL-25 is 5.3 times greater than that of Elekta Inor. On the other hand, the models Varian Clinac models show a considerably higher fluence than Elekta and Siemens in models of the same energy. In fact, the maximum fluence in Varian Clinac of 18 MV is 1.6 times larger than in Elekta SL-25 of 18 MV and 5.6 times higher than that found in the Siemens KDS of 18 MV. For energies of 15 MV, the maximum fluence found in the Varian Clinac is 3.7 times that found for the Elekta Inor.

The production of neutrons due to photons in each accelerator appears to be linked to the target materials and to a lesser extent, to the other elements in head. As shown in Table 1, the

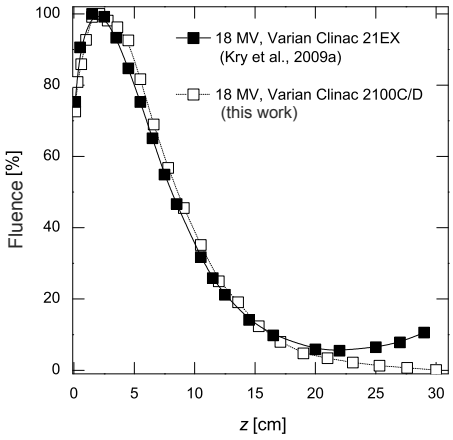

Figure 9. Comparison of the neutron fluence in a Varian Clinac 21EX accelerator of 18 MV [19] and the obtained for a Varian Clinac accelerator 2100 C/D, in this study.

target in the case of Varian Clinac is W, in the Siemens KDS is Au, while in Elekta is a mixture of W with other lighter elements. Moreover, the flattening filter in both the KDS as in Elekta models are made of lighter materials that filters of Varian. The jaws and multileaf include heavy materials in all the analyzed linacs.

Neutrons emitted from the target have average energies between 1 and 1.5 MeV. At these energies, the probability of neutron capture is negligible and neutrons mainly suffer elastic collisions (with Hydrogen), losing energy until they become thermal neutrons. Because of this, there is an increase of fluence to a maximun peak in the depth between 2-3 cm. When this maximum is reached, the neutron spectrum is more thermalized and begin to disappear by neutron capture processes, ^{14}N(n,p)^{14}C and ^{1}H(n,γ)^{2}H, much more likely at thermal energies, and the fluence decreases monotonically with depth. It can be considered that at $2-3$cm deep the net fluence decreases moderately and with a thickness of 7 and 10cm There is radiation to half, but there is also a certain dependence of the size of the phantom.

Fig. 9 compares the fluence for two different models of accelerators of the same mark, operated at 18 MV. On one side are the results of [19] for an accelerator Varian Clinac 21EX (black squares). With the results we have obtained here for the Varian Clinac 2100 C/D. Fluence values are normalized with respect to the maximum in both the cases.

The phantom used in the two calculations is ICRU tissue, of the same geometric characteristics, and we find, an agreement until 17 cm depth, in deeper points, near the base of the phantom, we observe an increase in the curve of [19]. This may be because their simulation includes the treatment table, and it can produce backscattering of neutrons in it, which could contribute to the total fluence in the deepest zone of the phantom.

4.2. ICRU phantom in front of a neutron source

Then we studied the behavior of the ICRU phantom in front of the neutron flux coming from the linacs. The effect can be studied if we calculate the spectra of fluence of neutrons just before the phantom and inside. A tally detector was located in air at 10 cm from the surface of

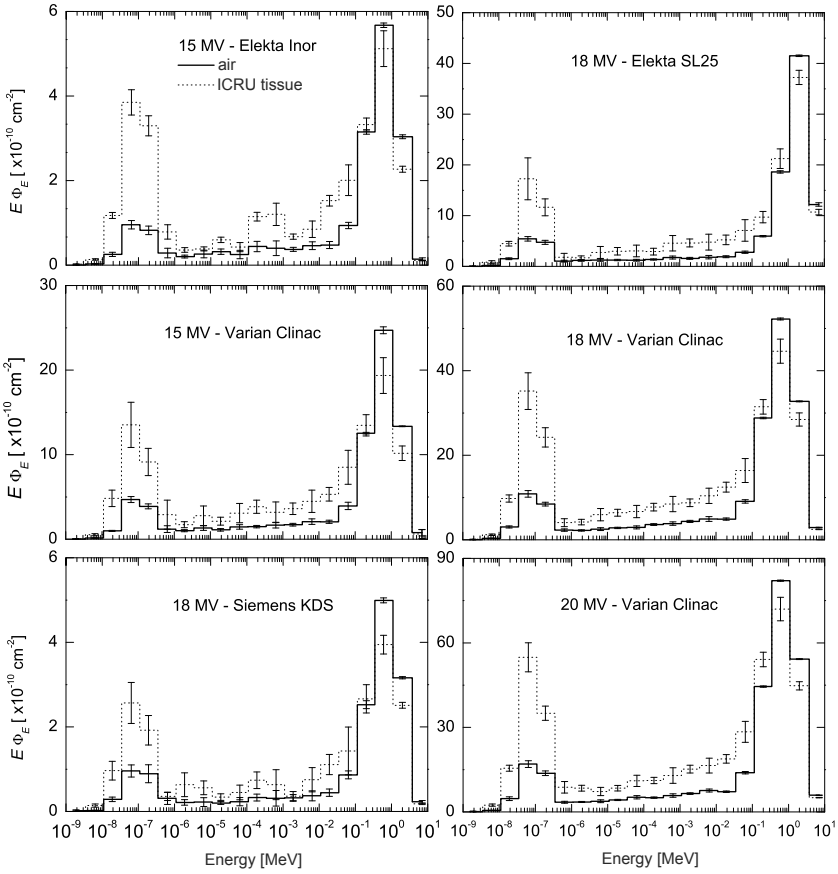

Figure 10. Spectrum of neutrons in air at 1 cm above the phantom (solid lines) and 1 cm inside the phantom (dotted lines).

the phantom, on the beam axis, and another at 1 cm into the phantom, also on the beam axis to achieve this end.

Energy spectra are shown in Fig. 10, wherein the histograms with solid lines correspond to the spectrum in air, while the histograms with dotted lines correspond to the spectrum within the ICRU tissue. We highlight some important aspects. It is observed in all cases that the peak is more pronounced at high energy and corresponds to the spectrum of fluence in air. This peak is due to fast neutrons that are emitted directly from the head of the linac.

The energy of these fast neutrons is within the energy range between 0.1 and 2 MeV proposed by [29] and [15] except the Elekta accelerator SL-25 of 18 MV, which emits neutron with energy significantly higher than the other accelerators studied.

It was also observed that at low energy, the thermal peak in tissue is greater than the thermal peak in air in all cases. This behavior is due to increased thermal neutrons that are caused by the interaction of fast neutrons primarily with the hydrogen the phantom. The thermal energy

range can be considered, according to Fig. 10, between 19 meV and 0.28 eV for all accelerators studied. Between the two peaks of neutron (thermal and fast), is find an epithermal neutrons spectrum that should not be neglected in the process of thermalization.

It is generally observed that, when passing from air into phantom, a significant decrease of fast neutrons and the increase in all cases of thermal neutron and epithermal neutrons accurs in all accelerators. It is concluded that phantom behaves as a moderador of neutrons due to its high content of ^{1}H, just 11.1% of total the ICRU phantom, with a threshold of thermal production of only 2.2 MeV [8].

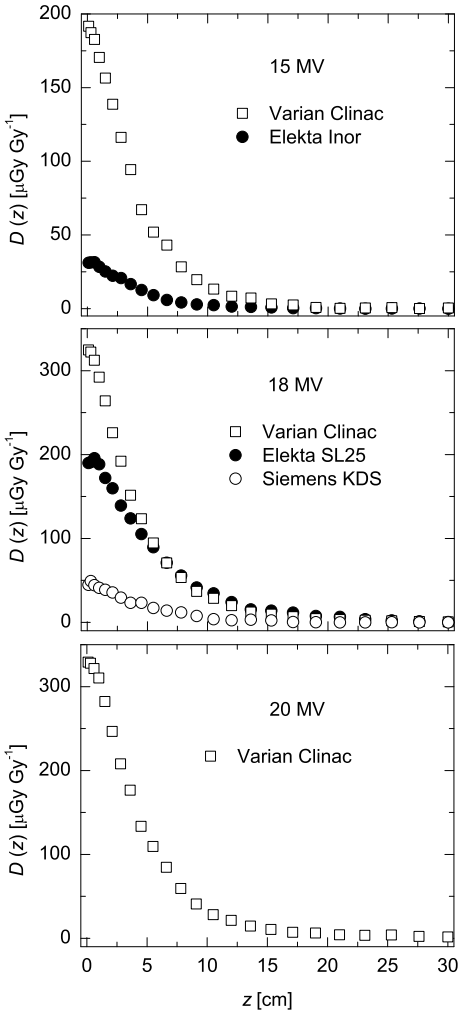

Figure 11. Absorbed dose due to neutrons as a function of depth in tissue ICRU for the different accelerators. The values are normalized to the maximum absorbed dose due to photons.

4.3. Absorbed dose due to neutrons

The radiation absorbed by the phantom ICRU, was calculated the kerma, which estimates the radiation absorbed by the medium, when exist balance of charged particles; in forward called absorbed dose, D.

The D due to neutrons was determined for all accelerators. The values obtained for the various configurations are shown in Fig. 11. The absorbed dose due to the neutrons in each case, is normalized to the maximum absorbed dose due to photons, however, we note that the absorbed dose in the Varian Clinac accelerator of 18 MV is slightly higher versus the Varian Clinac of 20 MV, although the flow is higher for the latter. This is because the values of absorbed dose due to neutrons are normalized to the maximum absorbed dose due to photons within the phantom.

The surface of phantom in Fig. 11, simulates the skin. The absorbed dose in each configuration is different according to this consideration. In the case of Varian of 15 MV this is 6.2 times greater than for Elekta Inor. The absorbed dose for Varian at 18 MV is 1.7 times greater than in the Elekta SL-25 and 7 times greater than the provided by Siemens KDS. The absorbed dose decreases with depth in all cases. To characterize this reduction, we determined depth in the tissue, at which the absorbed dose is reduced by 10% compared with the value in skin. For the Varian model, this depth is $\sim$ 9.5 cm, for Elekta models: $\sim$ 8.5 cm in the Inor linac and $\sim$ 12.5 cm for the SL-25. Finally, for the Siemens KDS it was found that this distance is $\sim$ 10 cm. These differences so marked are related, as we have been arguing, with high Z materials, used in the construction of equipment components, resulting in the generation of greater or lesser number of photonuclear reactions.

The absorbed dose decreases exponentially in the first 15 cm, in all cases, confirming that in a conventional treatment with a linear accelerator, the organs that are closer to the surface will receive a higher dose that the deeper organs.

4.4. Dose equivalent due to neutrons

The amount of radiation absorbed into tissue or organs may cause very different biological effects, and depends on the type of radiation or agent that produces particles, the value of the absorbed dose D is typically multiplied by the quality factors associated at the type of radiation, to find an equivalent in energy absorbed. The resulting quantity is called dose equivalent, H.

The dose equivalent is the amount that actually determines the biological damage to tissue or organs. The calculations of H are expressed in μSv·UM^{-1}, relative on the maximum absorbed dose due to photons that provides each accelerator in the region the build-up and then converted to Monitor Units (MU), where 1 MU = 1 cGy. According to [19], we have:

$$H = \sum_{E} D(E) \cdot Q_{\mathrm{n}}(E), \tag{1}$$

where $D(E)$, is the absorbed dose in tissue due to neutrons and calculated from the F6 tally ([33]), and $Q_{\mathrm{n}}(E)$ is the quality factor for neutrons of energy E in the corresponding material medium, in our case ICRU tissue [38]. H can also be calculated from the spectrum of fluence as:

$$H = \sum_{E} \Phi(E) \cdot k(E) \cdot Q_{\mathrm{n}}(E), \tag{2}$$

Where $\Phi(E)$ is the neutron fluence, calculated by F4 tally ([33]), $k(E)$ is the kerma factor for neutrons of energy E in tissue, calculated by [6], and $Q_{\mathrm{n}}(E)$ arequality factors for H, C, N, and O, calculated by [38]. The product $\Phi(E) \cdot k(E)$ represents the absorbed dose $D(E)$.

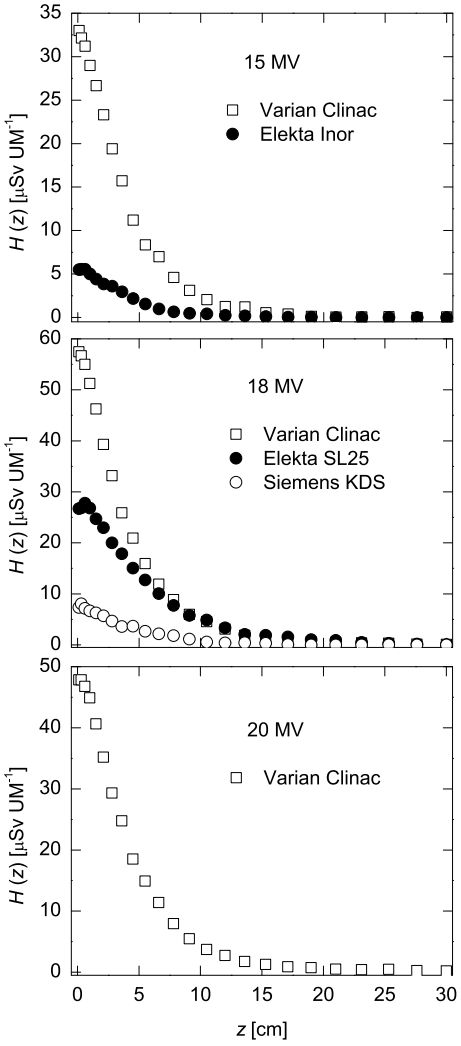

Figure 12. Dose equivalent per unit monitor in function of depth along the direction of the incident beam.

Fig. 12, shows the values of dose equivalent calculated for all accelerators studied, calculated with equation 1. If we consider the cell surface dimensions $2.0 \times 2.0 \times 0.1$ cm^3, which simulate the skin of thickness 0.1 cm, we can calculate the dose equivalent would receive this small portion of tissue, due to each accelerator which is 5.49, 7.34, 26.71, 33.01, 47.8 and 57.4 μSv·UM^{-1} for Elekta Inor, Siemens KDS, Elekta SL25 Varian Clinac de 15, 20 and 18 MV, respectively. As can be seen the highest value corresponds to the accelerator Varian Clinac 18

MV and the lowest for Elekta Inor accelerator followed Siemens KDS. It is further noted that $H(z)$ decreases significantly after 20 cm depth in all cases.

	$H(0)$ $[\mu\text{Gy} \cdot (\text{MU})^{-1}]$	λ $[\text{cm}^{-1}]$	χ^2 per d.o.f.
Varian Clinac 15 MV	37.0±0.9	0.263±0.007	1.45
Elekta Inor 15 MV	6.3±0.2	0.26±0.01	1.18
Varian Clinac 18 MV	64.0 ±1.0	0.251±0.004	1.52
Elekta SL25 18 MV	31.0±0.9	0.178±0.006	2.26
Siemens KDS 18 MV	8.5±0.3	0.224±0.009	0.95
Varian Clinac 20 MV	54.5±1.3	0.242± 0.006	2.81

Table 3. Values of the parameters of the fitting function 3 obtained for the dose equivalent values corresponding to the linacs analyzed in this work. The χ^2 per degree of freedom is also given.

The behavior shown by $H(z)$ depending on the depth on the phantom suggests an exponential dependence allowing a fit the data to a function of the form:

$$H(z) \;=\; H(0)\, \exp\left(-\lambda \cdot z\right), \tag{3}$$

where $H(0)$ is the maximum dose equivalent in surface and Z indicates the depth. The results of this adjustment are summarized in Table 3.

A first important aspect to note is the fact that the values of λ are quite similar in all cases, ranging between 0.178 and 0.263 cm^{-}1. Both $H(0)$ and λ coefficients depend on the primary spectrum of neutrons produced in first generation on the target and flattening filter of each linac by photon-neutron reactions, which in turn depends on the energy of electrons incident on the target and of course the components of the target. The coefficient λ depends of the phenomena the interaction of these primary neutrons with ICRU tissue, being predominant the elastic scattering on Hydrogen.

The cross section of elastic collision of the Hydrogen with the neutrons, depend inversely with of the energy themselves, being 0.3 cm^{-1} for 1 MeV, and between 0.1 and 0.2 cm^{-1} for 3 MeV. Note the similarity of these values with the coefficient λ which gives the fit for all the curves in Table 3.

The Fig. 13 compares the dose equivalent in depth obtained for three Varian accelerators operating at 18 MV: The Clinac 2100 C/D studied by us, the Clinac 21EX considered by [19] and a Varian generic simulated by [8] using a monoenergetic beam of neutron in direction perpendicular at phantom of water. Here the values of $H(z)$ are normalized to the maximum, H_{max}. As we see, our results (squares) are slightly on-top of the other authors in the area of intermediate depth, between 5 and 10 cm, approximately.

These differences may be related to the following motives: The accelerator studied by [19] is a Varian Clinac 21EX, equipped with a Millennium MLC of 120 sheets. In our case, the MLC is one of 80 sheets. But apart from this difference, the tuning energy used by [19] was 18.0 MeV, which differs from that set in our case (18.3 MeV). This difference in the energy of the initial electron, produce variations in the absorbed dose due to photons, and more specifically, its value at the isocenter, which, as already seen, can lead to differences in the values of H.

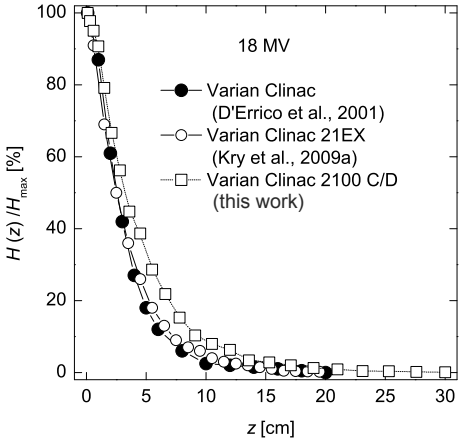

Figure 13. Comparison of the dose equivalent normalized to the maximum due to neutrons calculated in this study, with published results by [8] and [19].

The differences with the calculation of [8] are more evident due to that, as indicated; consider a monoenergetic beam of neutrons of 0.24 MeV. Both the material of phantom, and that is not considered the actual spectrum of the neutrons, are very outstanding aspects.

Now we analyze the profile of H outside the beam axis. This is important because, in a real treatment, the patient receive neutron radiation in all the body [25]. The Fig. 14 shows the results of dose equivalent profiles in function of distance from the central axis, at depths of 0.1 (open squares), 5.5 (dark squares), 10.5 (white circles) and 15.3 (black circles) cm, in the phantom ICRU for different accelerators studied.

In all cases, a general trend we observe: the dose equivalent decreases rapidly within a few inches away from the beam axis, to reach some uniformity. The region in which said reduction occurs depends on the type of accelerator, but is mainly related to the size of the radiation field. Indeed, an important part of H is transferred by neutrons with energies between 200 keV and the maximum available energy, 1-3 MeV. For distances larger than 5 cm off-axis beam (remember that the radiation field is the 10 cm^2), neutrons do not come directly to the phantom, but must pass through the jaws and in general the shield. This produces a reduction in its energy, which depend on the component materials of the head and the distance that must to traverse through within these materials. In the case of Elekta accelerators, the dose equivalent is increased at a distance exceeding 30 cm off-axis, which does not occur in other accelerators, at least as clearly. It should be noted here, that the Elekta accelerators analyzed have a flattening filter double, to which is added the fact that also a part of their secondary collimating system is oriented perpendicularly to the axis of radiation (see Fig. 2), which does not occur with the other accelerators. In conclusion the dose equivalent tends to be much more uniform and smaller, when increases the depth in the phantom. This is an important aspect to be taken into account for calculating the dose equivalent in organs [25].

4.5. Comparison of simulations and experimental measurements

If we analyze the Monte Carlo calculations and the experimental measurements, we observed differences that can be explained, taking into account the major problems when measuring

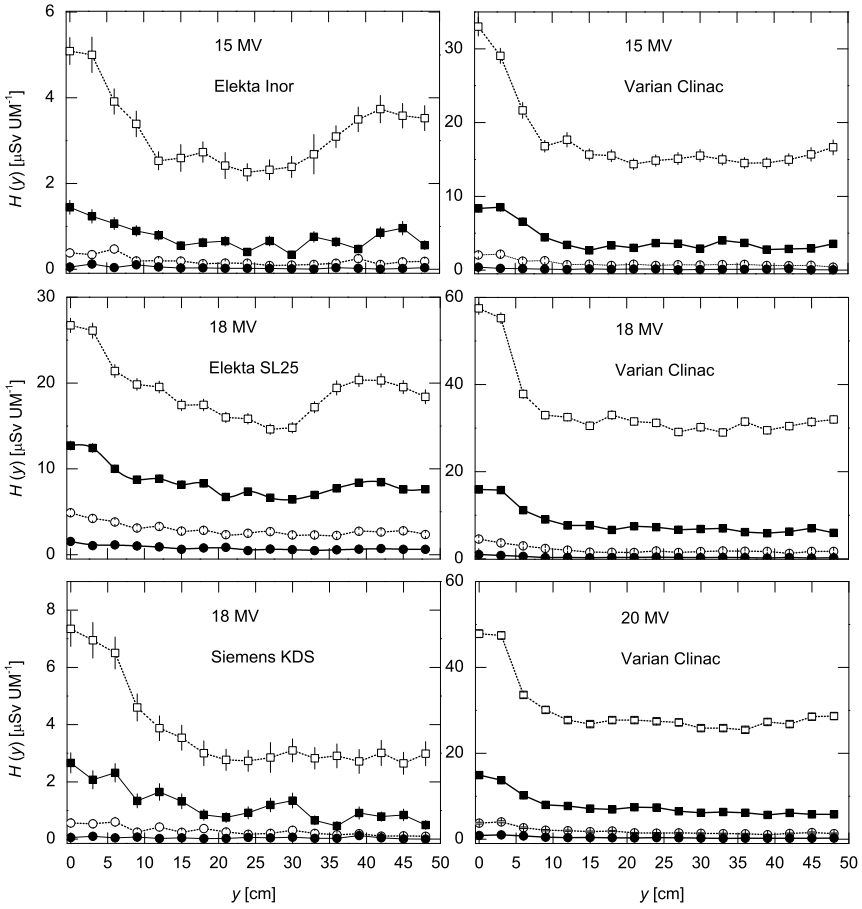

Figure 14. The profiles H to depths of 0.1 (open squares), 5.5 (dark squares), 10.5 (white circles) and 15.3 (dark circles) cm, inside the phantom, in direction transverse to the beam axis.

the neutron fluence. The sensitivity of the detectors used depends significantly on the neutron energy and this greatly influences the experimental measured of dose equivalent H.

The Fig. 15 compares experimental measurements of H, made with bubble detectors and detectors based on the CR-39 polymer by [21] and [8, 9] in water, with calculations of dose equivalent by Monte Carlo in function of depth and in the direction of central axis. The lower panel shows the results for 18 MV accelerators, together with the results obtained in our calculations for the Varian Clinac accelerators, Elekta SL 25 and Siemens KDS, in the top panel the corresponding to accelerators of 15 MV. For the Siemens Primus accelerator of 15 MV, it is observed that measures of [21] in surface are similar to the results of the calculations for the Varian Clinac of 15 MV in this work; but with increasing depth, these experimental results show much higher values than those obtained by [8, 9], which are more consistent with Monte Carlo calculations performed in this work, especially for 15 MV.

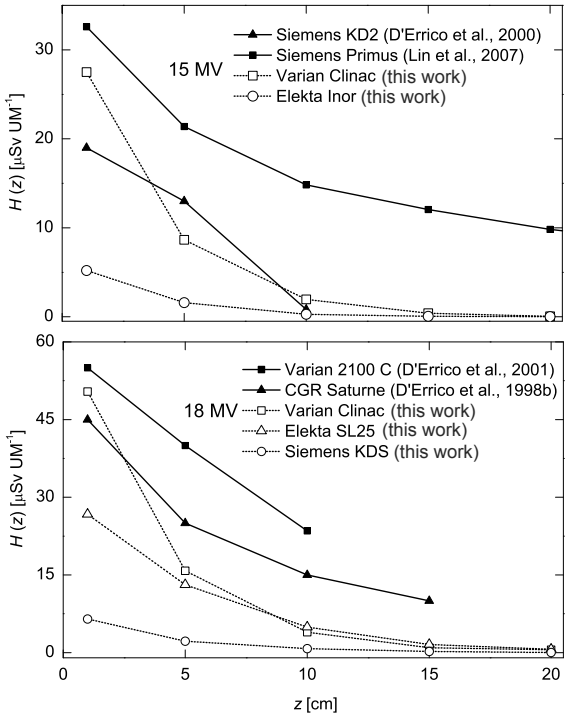

Figure 15. Dose equivalent H in function of the depth, calculated in accelerators of 15 and 18 MV, compared with measurements on a Siemens Primus of 15 MV [21], a Siemens KD-2 of 15 MV and a Varian Clinac 2100 C of 18 MV [8] and a CGR Saturne of 18 MV [9].

This is the general situation for all employees measurement systems for neutrons, without having to date, the ideal detector that can respond at any desired energy range. This is where Monte Carlo once again becomes the tool adequate for such studies.

In Fig. 16 we compared profiles dose equivalent $H(y)$ measured and calculated in this study, in function on the distance to the axis of incidence and for several accelerator of 15 MV (top panel) and 18 MV (bottom panel). The behavior of the profile of $H(y)$ is very similar in all cases, with rapid decrease in the first 10 cm, from which have small variations, except in the accelerators Siemens KDS 18 MV and Elekta Inor of 15 MV, due to low production of photoneutrons, as demonstrated above. In the top panel of Fig. 16 shows some agreement between the experimental results for the Siemens Primus accelerator and simulations for the accelerator Varian Clinac analyzed in this study.

This suggests that the bubble detectors BD-PND used have an acceptable response in surface, as mentioned before, which does not occur with BDT bubble detectors used in depth for the measurement of thermal neutrons by [21]. In general, we see that from the 10 cm off axis, $H(y)$ has small variations, very similar behavior to that found in the studied profiles in Fig. 16.

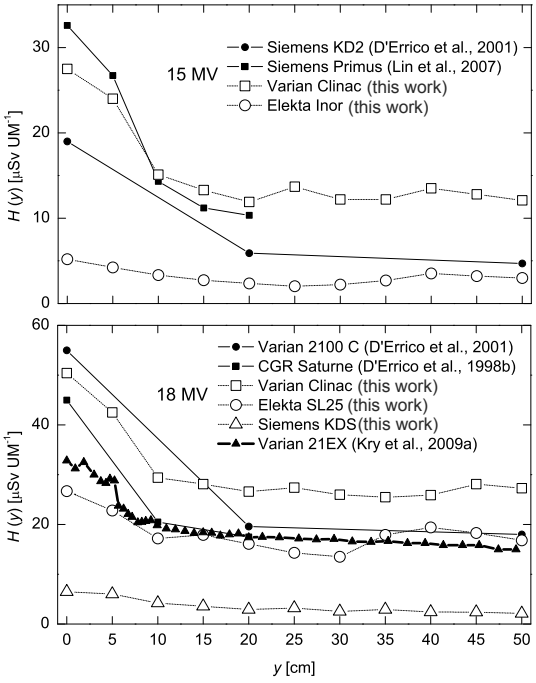

Figure 16. Profiles of dose equivalent to $Z = 1$ cm into the phantom ICRU, as function of the distance transverse to the beam axis, for linacs of 15 and 18 MV, compared with measurements of a Siemens Primus of 15 MV [21], a Siemens KD-2 of 15 MV [8], a Varian Clinac 2100 C of 18 MV [8] and a CGR Saturne of 18 MV [9] and calculations for a Varian Clinac 21EX of 18 MV [19].

5. Conclusions

In this work, the photoneutron production in four linacs with a total of six energy configurations has been analysed using the Monte Carlo code MCNPX. A detailed simulation of the geometries of the linac head has been carried out. The aim was to study the neutron dose equivalent in patients treated with these linacs in order to compare the differences between them. The important point was that the same methodology was used in all the cases, something not done till now for some of the quantities of interest here analysed.

A first result to be pointed out concerns the considerably larger photoneutron production of the Varian Clinac 2100C in comparison with the Elekta Inor and SL-25 and the Siemens Mevatron KDS for the same energy. This larger production can be linked to the materials used to built-up the target in each specific linac. In any case, the maximum fluences observed for the various linacs show a dependence almost linear with the tuned energies of the electrons incident in the target.

Neutron spectra in air, nearby the phantom and at a depth of 1 cm in the phantom were calculated. In air, the spectra are characterised, in all cases, by a pronounced peak at high energy (200 keV to 3 MeV). This peak reduces notably inside the phantom, where a peak at thermal energies appears due to neutron moderation by the medium.

Absorbed doses and dose equivalent show a similar behaviour, as a function of the depth in the phantom: they reduce strongly with the depth. This reduction can be reproduced by means of an exponential function in which the reduction rate, obtained after the corresponding fit procedure, is closely related to the cross section for elastic neutron with Hydrogen collisions at the maximum energies present in the neutron spectra obtained in the simulations.

The trend of the dose equivalent values, as a function of the transverse axis distance to the beam axis, depends strongly on the radiation field used. For large distances to the beam axis, these doses are uniform, except for the Elekta Inor and SL-25 accelerators in which they grow up. This is linked to the material present in the secondary collimators of the linacs.

One of the main points of our work concerns the determination of the dose equivalent due to neutrons inside the phantom. This has permitted to gain insight about the dose distribution in patients submitted to radiotherapy with photon beams 15 MV. As a result, it was found that surface organs are the most affected by the overdose produced by neutrons.

Author details

S. Agustín Martínez Ovalle
Universidad Pedagógica y Tecnológica de Colombia, Group of Applied Nuclear Physics and Simulation, Colombia

6. References

[1] AAPM-19 [1986]. American Association of Physicists in Medicine, *Report 19* .
[2] Agostinelli, S. e. a. [2003]. Geant4-a simulation toolkit, *Nuclear Instruments and Methods in Physics Research A* 506: 250–303.
[3] Barquero, R., Edwards, T. M., Iniguez, M. P. & Vega-Carrillo, H. R. [2005a]. Monte Carlo simulation estimates of neutron doses to critical organs of a patient undergoing 18 MV x-ray LINAC-based radiotherapy, *Medical Physics* 32: 3579–3588.
[4] BJR-25, [1996]. Central axis depth dose data for use in radiotherapy : a survey of depth doses and related data measured in water or equivalent media / prepared by a Joint Working Party of the British Institute of Radiology and the Institution of Physics and Engineering in Medicine and Biology, *British Journal of Radiology*.
[5] Briesmeister, J. F. [2000]. MCNP-A General Monte Carlo N-Particle Transoprt Code, Version 4C., *Los Alamos National Laboratory* Report: LA–13709–M.
[6] Caswell, R. S., Coyne, J. J. & Randolph, M. L. [1980]. Kerma factors for neutron energies below 30 MeV, *Radiaton Research* 83: 217–254.
[7] Chibani, O. & Ma, C. C. [2003]. Photonuclear dose calculations for high energy photon beams from Siemens and Varian linacs, *Medical Physics* 30: 1990–2000.
[8] D'Errico, F., Luszik-Bhadra, M. & Nath, R. [2001]. Depth dose equivalent and effective energies of photoneutrons generated by 6-18 MV X-ray beams for radiotherapy, *Health Physics* 80: 4–11.
[9] D'Errico, F., Nath, R., Tana, L., Curzio, G. & Alberts, W. G. [1998]. In-phantom dosimetry and spectrometry of photoneutrons from an 18MV linear accelerator, *Medical Physics* 25: 1717–1724.
[10] Followill, D. S., Stovall, M. S., Kry, S. F. & Ibbott, G. S. [2003]. Neutron source strength measurements for Varian, Siemens, Elekta, and General Electric linear accelerators, *Journal of Applied Clinical Medical Physics* 4: 189–194.

[11] Harrison, R. M., Wilkinson, M., Shemilt, A., Rawlings, D. J., Moore, M. & Lecomber, A. R. [2006]. Organ doses from prostate radiotherapy and associated concomitant exposures, *British Journal of Radiology* 79: 487–496.
[12] Howell, R. M., Hertel, N. E., Wang, Z., Hutchinson, J. & Fullerton, G. D. [2006]. Calculation of effective dose from measurements of secondary neutron spectra and scattered photon dose from dynamic MLC IMRT for 6 MV, 15 MV, and 18 MV beam energies, *Medical Physics* 33: 360–368.
[13] Howell, R. M., Kry, S. F., Burgett, E., Hertel, N. E. & Followill, D. [2009]. Secondary neutron spectra from modern Varian, Siemens, and Elekta linacs with multileaf collimatorss, *Medical Physics* 36: 4027–4038.
[14] IAEA-398 [2000]. International Atomic Energy Agency, Absorbed dose determination in external beam radiotherapy: An international code of practice for dosimetry based on standards of absorbed dose to water, *Report 398* .
[15] ICRU-40 [1986]. International Commission on Radiation Units and Measurements. The Quality Factor in Radiation Protection, *Report 40* .
[16] ICRU-44 [1989]. International Commission on Radiation Units and Measurements. Tissue substitutes in radiation dosimetry and measurement, *Report 44* .
[17] IPSM-35 [1990]. Institute of Physical Sciences in Medicine, Code of practice for high-energy photon therapy dosimetry based on the NPL absorbed dose calibration service, *Physics in Medicine and Biology* 35: 1355–1360.
[18] Kase, K. R., Mao, X. S. & Nelson, W. R. [1998]. Neutron fluence and energy spectra around the Varian Clinac 2100C/2300C medical accelerator, *Health Physics* 74: 38–47.
[19] Kry, S. F., Howell, R. M., Salehpour, M. & Followill, D. [2009]. Neutron spectra and dose equivalents calculated in tissue for high-energy radiation therapy, *Medical Physics* 36: 1244–1250.
[20] Lin, J. P., Chu, T. C., Lin, S. Y. & Liu, M. T. [2001]. The measurement of photoneutrons in the vicinity of a Siemens Primus linear accelerator, *Applied Radiation and Isotopes* 55: 315–321.
[21] Lin, J. P., Liu, W. C. & Lin, C. C. [2007]. Investigation of photoneutron dose equivalent from high-energy photons in radiotherapy, *Applied Radiation and Isotopes* 65: 599–604.
[22] Ma, A., Awotwi-Pratt, J., Alghamdi, A., Alfuraih, A. & Spyrou, N. M. [2008]. Monte Carlo study photoneutron production in the Varian Clinac 2100c linac, *Journal of Radioanalytical and Nuclear Chemistry* 276: 119–123.
[23] Mao, X. S., Kase, K. R., Liu, J. C., Nelson, W. R., Kleck, J. H. & Johnsen, S. [1997]. Neutron sources in the varian clinic 2100C/2300C medical accelerator calculated by the EGS4 code, *Health Physics* 72: 524–529.
[24] Martínez, S. A., Barquero, R., Gómez Ros, J. M. & Lallena, A. M. [2011]. Neutron dose equivalent and neutron spectra in tissue for clinical linacs operating at 15, 18 and 20 MV, *Radiation Protection Dosimetry* p. doi:10.1093/rpd/ncq501.
[25] Martínez, S. A., Barquero, R., Gómez Ros, J. M. & Lallena, A. M. [2012]. Neutron dosimetry in organs of an adult human phantom using linacs with multileaf collimator in radiotherapy treatments, *Medical Physics* 39: 2854–2866.
[26] Martínez, S. A., Barquero, R., Gómez Ros, J. M., Lallena, A. M., Andrés, C. & Tortosa, R. [2010]. Evaluation of neutron production in new accelerator for radiotheraphy, *Radiation Measurements* 45: 1402–1405.
[27] McCall, R. C., Jenkins, T. M. & Shore, R. A. [1979]. Transport of accelerator produced neutrons in a concrete room, *IEE Transactions on nuclear Science* NS-26: 1593–1602.
[28] Mesbahi, A. [2006]. Development a simple point source model for Elekta SL-25 linear accelerator using MCNP4C Monte Carlo code, *Iranian Journal of Radiation Research* 4: 7–14.

[29] NCRP-79 [1984]. National Council on Radiation Protection and Measurements. Neutron contamination from medical electron accelerators, *Report 79* .
[30] Nelson, W. R., Hirayama, H. & Rogers, D. W. [1987]. The EGS4 code system, *National Accelerator Laboratory* p. SLAC Report 265.
[31] Ongaro, C., Nastasi, U. & Zanini, A. [1999]. Monte Carlo simulation of the photo-neutron production in the high-Z components of radiotherapy linear accelerators, *Monte Carlo Methods Applied* 5: 69–79.
[32] Ongaro, C., Zanini, A., Nastasi, U., Rodenas, J., Ottaviano, G. & Manfredotti, C. [2000]. Analysis of photoneutron spectra produced in medical accelerators, *Physics in Medicine and Biology* 45: L55–L61.
[33] Pelowitz, D. B. [2005]. MCNPX User's Manual Version 2.5.0, *Los Alamos National. Laboratory* pp. Report LA–UR–02–2607.
[34] Pena, J., Franco, L., Gómez, F., Iglesias, A., Pardo, J. & Pombar, M. [2005]. Monte Carlo study of Siemens PRIMUS photoneutron production, *Physics in Medicine and Biology* 50: 5921–5933.
[35] Reft, C. S., Runkel-Muller, R. & Myrianthopoulos, L. [2006]. In vivo and phantom measurements of the secondary photon and neutron doses for prostate patients undergoing 18 MV IMRT, *Medical Physics* 33: 3734–3742.
[36] S. A. Martínez Ovalle, J. M. Gómez Ros, A. M. L. R. [2011]. *Estudio Monte Carlo de la dosimetría de fotoneutrones producidos en aceleradores de uso clínico*, Documentos CIEMAT.
[37] Saeed, M. K., Moustafa, O., Yasin, O. A., Tuniz, C. & Habbani, F. I. [2009]. Doses to patients from photoneutrons emitted in a medical linear accelerator, *Radiation Protection Dosimetry* 133: 130–135.
[38] Schuhmacher, H. & Siebert, B. R. L. [1992]. Quality factors and ambient dose equivalent for neutrons based on the new ICRP recommendations, *Radiation Protection Dosimetry* 40: 85–89.
[39] Schulz, R. J., Almod, P. R., Cunningham, J. R., Garrett Holt, J., Loevinger, R., Suntharalingam, N., Wright, K. A., Nath, R. & Lempert, G. D. [1983]. American Association of Physicists in Medicine, A protocol for the determination of absorbed dose from high-energy photon and electrons beams, *Medical Physics* 10: 741–771.
[40] Vanhavere, F., Huyskens, D. & Struelens, L. [2004]. Peripheral neutron and gamma doses in radiotherapy with an 18 MV linear accelerator, *Radiation Protection Dosimetry* 110: 607–612.
[41] Zanini, A., Durisi, E., Fasolo, F., Ongaro, C., Visca, L., Nastasi, U., Burn, K. W., Scielzo, G., Adler, J. O., Annand, J. R. M. & Rosner, G. [2004a]. Monte Carlo simulation of the photoneutron field in linac radiotherapy treatments with different collimation systems, *Physics in Medicine and Biology* 49: 571–582.
[42] Zanini, A., Durisi, E., Fasolo, F., Visca, L., Ongaro, C., Nastasi, U., Burn, K. W. & Annand, J. R. M. [2004b]. Neutron spectra in a tissue equivalent phantom during photon radiotherapy treatment by linacs, *Radiation Protection Dosimetry* 110: 157–160.